01 Jan 2017

Retarding Field Energy Analyzer for High Energy Pulsed Electron Beam Measurements

J. Hu

Joshua L. Rovey
Missouri University of Science and Technology, roveyj@mst.edu

W. Zhao

Recommended Citation

J. Hu et al., "Retarding Field Energy Analyzer for High Energy Pulsed Electron Beam Measurements," *Review of Scientific Instruments*, vol. 88, no. 1, American Institute of Physics (AIP), Jan 2017.
The definitive version is available at https://doi.org/10.1063/1.4973776

Retarding field energy analyzer for high energy pulsed electron beam measurements

Jing Hu,[1,a)] Joshua L. Rovey,[2] and Wansheng Zhao[1]
[1]*State Key Laboratory of Mechanical System and Vibration, Mechanical Engineering Department, Shanghai Jiao Tong University, Shanghai 200240, People's Republic of China*
[2]*Department of Mechanical and Aerospace Engineering, Missouri University of Science and Technology, Rolla, Missouri 65409, USA*

(Received 9 April 2016; accepted 26 December 2016; published online 17 January 2017; corrected 26 January 2017)

A retarding field energy analyzer (RFEA) designed specifically for high energy pulsed electron beam measurements is described in this work. By proper design of the entrance grid, attenuation grid, and beam collector, this RFEA is capable of determining the time-resolved energy distribution of high energy pulsed electron beams normally generated under "soft vacuum" environment. The performance of the RFEA is validated by multiple tests of the leakage current, attenuation coefficient, and response time. The test results show that the retarding potential in the RFEA can go up to the same voltage as the electron beam source, which is 20 kV for the maximum in this work. Additionally, an attenuation coefficient of 4.2 is obtained in the RFEA while the percent difference of the rise time of the electron beam pulse before and after attenuation is lower than 10%. When compared with a reference source, the percent difference of the RFEA response time is less than 10% for fall times greater than 35 ns. Finally, the test results of the 10 kV pseudospark-based pulsed electron beam currents collected under varying retarding potentials are presented in this paper. *Published by AIP Publishing.* [http://dx.doi.org/10.1063/1.4973776]

I. INTRODUCTION

Novel methods for the surface treatment of metallic materials by pulsed concentrated energy fluxes have been intensely developed in recent decades, including laser beams, and ion and electron beams. In the surface treatment process via pulsed energetic beams, the repetitive beam energy flux causes superfast heating, melting, and evaporation of the surface layer. Then the physical and mechanical properties of the material can be altered by producing the metastable states via the superfast "heating-melting-solidification" processes.[1–8] Compared with pulsed laser beams, high-power charged particles, such as ion and electron beams, are more favorable for surface treatment applications, mainly due to their high efficiency of incident energy absorption carried by the beam. In Refs. 4–8, pulsed electron beams of high current densities (10^2–10^3 A/cm^2), high energies (10–40 keV), and short pulse durations (10^{-8}–10^{-6} s) have been validated for a variety of metal and alloy surface treatments, including alloying, nitriding, and polishing.

Being an exceptionally efficient method of material processing, determination of the beam energy and distribution are of great importance to determine the energy delivery in the interaction between the beam and material surface, and evaluate the beam quality and optimize the parameters of the electron beam source for material processing. In some previous research work, the average energy of high energy pulsed electron beams was evaluated by various methods,[9–12] such as x-ray radiation method[9–11] and electron range-energy study method by stopping foils of varying thicknesses.[12] However, in addition to the evaluation of mean energy of the pulsed electron beam via a variety of experimental methods, only a few studies have focused on the determination and construction of time-resolved energy distributions of high energy pulsed electron beams for material processing, which are of great interest in material processing applications.[1,2,6,13–15] For example, the detailed temporal evolution of the electron energy distribution is essential for understanding and monitoring the dynamic heating process and energy delivery pattern of the input beam flux on the material surface.[6,13–15] The common experimental methods to determine the time-resolved energy distribution of electron beam, such as retarding field energy analyzer (RFEA), are suitable for the measurement of low energy and DC electron beams. However, due to several unique features and limitations of both normal RFEA and beam parameters, it is difficult to measure the time-resolved energy distribution of high energy pulsed electron beams as discussed below.

The most common method to obtain the time-resolved energy distribution of charge particles (including both ions and electrons) is RFEA, consisting of an electron beam collector, retarding and grounding grids to form the retarding field, and ground housing if required, as shown in Figure 1. Charged particles, either ions or electrons, originate at the source and travel towards the retarding grid. A retarding potential, V_r, is applied to the retarding grid to decelerate the electrons. Only the electrons with energy higher than the value of eV_r, where e is the single electron charge, can pass through the retarding potential and be collected by the electron beam collector in the downstream direction of RFEA. When varying the retarding potential to different values of $V_r(i)$, a series of electron beam current pulses are collected as $I(\epsilon_i, t)$, where $\epsilon_i = eV_r(i)$ represents the electron energy. Thus the numbers of electrons

a)Electronic mail: jhgdb@sjtu.edu.cn

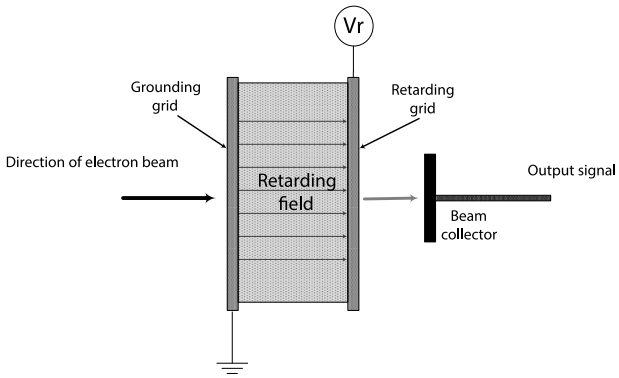

FIG. 1. Schematic of the retarding field energy analyzer (RFEA).

of varying energy values over the electron pulse duration t can be determined by varying the applied retarding potential. A detailed description of RFEA operation principles has been presented and discussed thoroughly in Refs. 16 and 17. RFEA has been used extensively for the accurate measurement of ion and electron currents and determination of the ion and electron energy distributions in plasma, with typical energy ranging from several eV to tens of eV.[18–22] However, as presented above, the electron beams for material processing are characterized on the time scale of 10^{-9}–10^{-6} s, peak energies of keV, energy densities of 1–40 J/cm^2, and current densities of 10^3 A/cm^2,[7,8,23–25] which will cause several challenges in the RFEA described next.

A. Retarding potential limits

Determination of the full spectrum of the electron beam energy requires that the retarding potential is varied from 0 V to the peak value of acceleration potential of the electron beam source. However, pulsed electron beams of keV are generated under the "soft vacuum" pressure ranging from tens of mTorr to hundreds of mTorr,[4–8,10–15] which is located at the minimum zone of the Paschen curve and has very low breakdown voltage (several hundred volts), mainly due to the complicated gas breakdown processes in soft vacuum dominated by both stationary field emission and nonstationary processes including the electron explosive emission and vacuum spark, multipactor discharge, etc.[16,17,28] Thus it is difficult for the retarding potential to go up to several kV to tens kV without causing undesired gas breakdown and associated leakage current between the retarding and grounding grids.

B. Space-charge limit of the high beam current densities

High current and current density are two major characteristics of the high energy pulsed electron beams favorable for material processing. However, due to the high current density of the pulsed electron beam, the impact of incomplete space charge neutralization in the RFEA under the high current densities can affect the construction of the electron beam energy spectrum due to the formation of a virtual cathode, which has been discussed thoroughly in Ref. 17. Thus the proper attenuation of the RFEA should be considered and designed with specific caution.

C. Fast response time of the RFEA

Different from dc-beams without time structure, pulsed electron beams for material processing are normally characterized on the time scale of 10^{-9}–10^{-7} s. Under such time scale, the physical dimension of the beam measurement system is comparable with the signal wavelength of electron beam pulse, which means that the pulse measurement system should be treated as a transmission line instead of lumped elements.[26] Thus special attention is required for the design of the electron beam collector in the RFEA to minimize its stray inductance and response time.

In this work, an improved RFEA specifically designed for the measurement of high energy pulsed electron beams is presented. Details are given on how the design problems are removed with careful considerations and determinations of the grid attenuation, shielding and grounding, and the elimination of the gas breakdown and associated current caused by the high retarding potential in the RFEA. This paper is organized into the following sections: In Sec. I, a detailed introduction to the unique properties of high energy pulsed electron beams, and the challenges and limitations to determine the energy distribution are presented. The design procedures of the RFEA and the experimental setup are shown in Sec. II. The performance validation test results of the RFEA and the measurement results of the time-resolved pulsed electron beam energy are shown in Sec. III. Finally, the conclusions and discussions are summarized in Sec. IV.

II. DESIGN PROCEDURE AND EXPERIMENTAL SETUP

The RFEA presented in this work is designed for the pulsed high energy electron beams generated by a transient hollow cathode discharge (THCD) device named pseudospark, which consists of a hollow cathode, an exit anode, and multiple intergaps as illustrated in Figure 2. The typical waveforms of the pseudospark voltage and discharge current are illustrated in Figure 3, with the oscillation caused by the inductance of the discharge chamber loop. The THCD-based electron beam is characterized by short duration (tens to hundreds of nanoseconds), high peak energy (hundreds of eV to tens of keV), and high beam current (tens of A to kA), which make it favorable for a variety of material processing applications.[4–6,9,10,13,17,18]

The improved RFEA designed for the pseudospark-based high energy electron beam measurements is sketched in Figure 4. As illustrated in Figure 4, the RFEA consists of an electron collector, an entrance grid working as a pressure insulator between regions I and II, attenuation grid, and the electromagnetic shielding. The detailed design principles of each part are discussed in this section.

A. Design of the entrance grid

As discussed in Sec. I A, within the operating pressure range of THCD-based electron beam (10-100 mTorr), gas breakdown is easily formed under tens of kV retarding potentials (even several kV) between the retarding grid and ground of the RFEA, which makes the regular RFEA fail to work for the high energy electron beam measurements. In order to

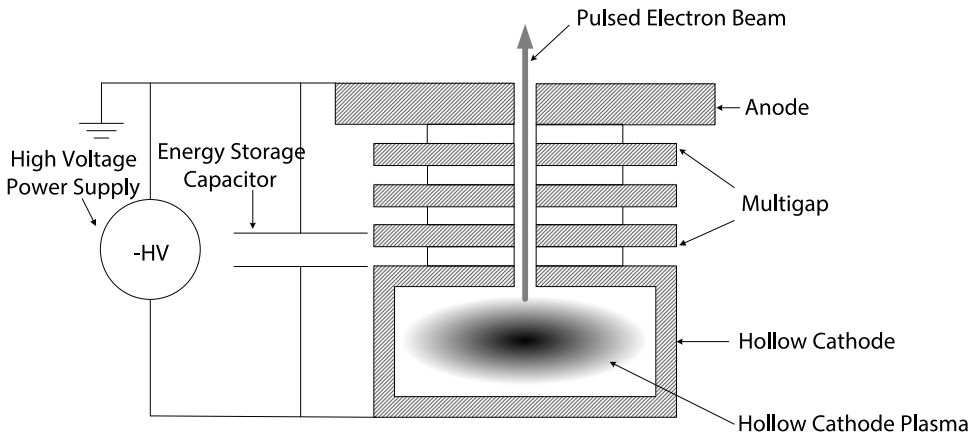

FIG. 2. Multigap pseudospark-based chamber for the pulsed electron beam generation.

eliminate this gas breakdown, an entrance grid with a central orifice to form a pressure gradient is located in front of the electron collector, which isolates the THCD operation region (region I) and electron beam drift region (region II). In the molecular flow region, which is dominant at high and ultra-high vacuum, the flow conductance is independent of pressure but dependent on the geometry of the conductance pipelines. Thus for a thin aperture whose diameter exceeds its length as presented in this work,[27]

$$C = 3.7 \times (\frac{T}{M})^{1/2} \times A, \quad (1)$$

where A is the area in cm^2 and conductance is in L/s. Thus compared with region I of 5 cm internal tube diameter, an entrance grid with a 2 mm diameter orifice located in front of region II is capable of forming a scaling factor of 10^4 between the conductance of regions I and II. As a result of such a high vacuum conductance difference, a pressure gradient is formed between regions I and II under the given pumping time. When the pressure in region I has to be maintained at the operational pressure range of THCD-based electron beam source (10^{-1}–10^{-2} Torr), the pressure in region II can be evacuated and maintained at 10^{-4}–10^{-5} Torr. In such a high vacuum in region II, the electron mean free path for ionization, which is typically tens of centimeters, is much greater than the spacing between the grounding and retarding grids. In such a region, only a small part of the total electron flow ionizes the gas.[28,29] Thus region II is within the pressure range for vacuum breakdown which has a very high breakdown voltage (normally higher than 30 kV[30]). The retarding potential can then be increased to the required values (<20 kV) without gas breakdown occuring within the RFEA.

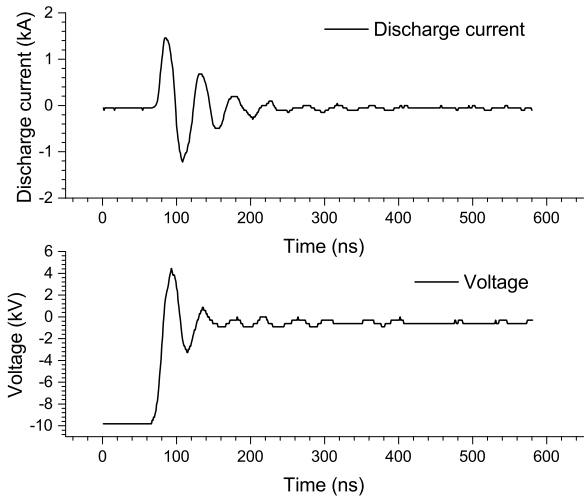

FIG. 3. Breakdown voltage and discharge current of the multigap pseudospark-based chamber.

B. Design of the attenuation grid

As discussed in Section I, a proper attenuation grid is required to reduce the electron beam current density below the space-charge limit. The attenuation coefficient of the grid is determined by the limiting value given by the Child-Langmuir law,[31]

$$I_{Lim} = J_{Lim} \times S = \frac{4\varepsilon_0}{9}\sqrt{\frac{2e}{m_e}}\frac{U^{3/2}}{d^2} \times S, \quad (2)$$

where S is the area of beam cross sections, U is the applied voltage, and d is the distance in the electron beam source. According to Equation (2), the space-charge limited current, which is equal to 1.9 A at 10 kV in the presented RFEA setup with a 1 mm beam radius and 2 mm distance between the grounded attenuation grid and retarding grid. In addition to the proper attenuation coefficient to lower the beam current density below the space-charge limited value, the possible uniform decrease in the electron density caused by a large attenuation coefficient is also an important factor to determine the attenuation grid design. Thus in this work, the attenuation of high current density is obtained by both the attenuation grid with 55% grid transmission and the orifice in the entrance grid. In addition, the attenuation grid is connected to the diagnostic room ground which envelops the analyzer as illustrated in Figure 4, in order to provide the required electromagnetic shielding and grounding.

C. Design of the electron beam collector

In our work, a Faraday Cup (FC) probe is selected to be the pulsed electron beam collector due to the simple configuration

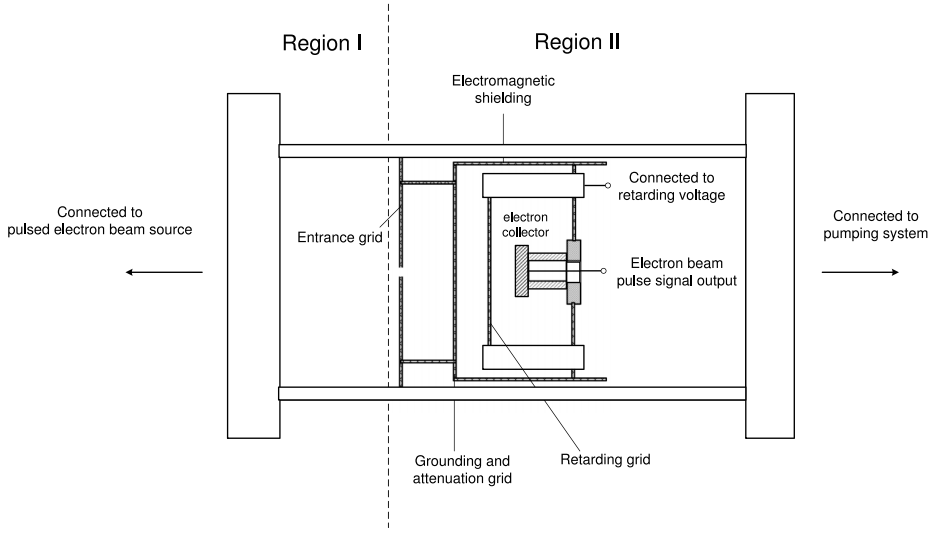

FIG. 4. The RFEA for high energy pulsed electron beam measurements.

and large measurement range. The FC probe in our work is developed to stop and measure 20 keV, 1 nC electron pulse beam. Based on the beam properties, the low inductance and fast response time are two major issues in our FC probe design. As illustrated in Figure 5, this FC probe is constructed based on a semi-rigid coaxial cable with 50 Ω impedance which has the similar structure as the FC presented in Ref. 32, consisting of a copper collector cup to capture the electron beam, the grounding plate and a carbon resistor connected between the copper collector and grounding plate serve as the shunt resistor. The inner conductor of this coaxial cable is joint with the copper collector cup. The coaxial cable insulated with Teflon coating is passed through the center of the carbon resistor, and the outer grounding mesh of the coaxial cable is connected to the grounding plate. The other side of this semi-rigid coaxial cable is soldered into an N type coaxial connector. Then a low shunt resistance can be formed between the collector and grounding plate as a compact configuration with minimum stray inductance and reflection of pulse signal.

D. Experimental setup

The experimental setup for the generation and measurement of the pseudospark-based electron beam as well as the performance validation test system is shown in Figure 6. This pseudospark-based electron beam experiment has also been used and is described in our previous research.[32,33] The experimental setup consists of two sections: The left side is the multigap pseudospark discharge section, including a 16-gap pseudospark discharge device. A hollow cathode is connected to the high voltage dc power supply (100 kV, 1 mA) through a 20 MΩ charging resistor. Two 700 pF resin-dipped ceramic capacitors were connected between the anode and cathode symmetrically for energy storage. A custom North Star high voltage probe PVM-5 is connected to the cathode to measure the voltage breakdown waveform.[34]

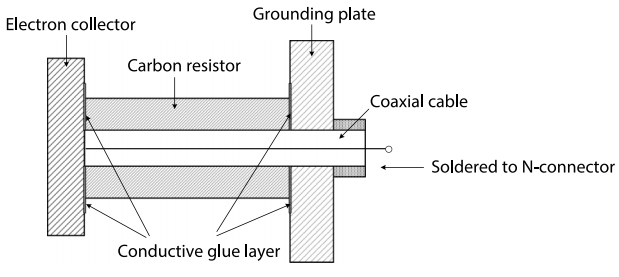

FIG. 5. FC probe with low inductance and shunt resistance.

The improved RFEA for the pseudospark-based electron beams is located on the right side in Figure 6, including the electron beam detector, multiple grids, and electromagnetic shield. In our research work, the electron beam detectors include a Rogowski coil with a response time of 4 ns (current transformer NO.2 in Figure 6) and the low resistance FC probe presented in Section II C. In the performance validation tests of the FC probe, the current transformer NO.2 is connected with the same pulse generator as the FC probe to determine and calibrate the resistance of FC probe in this work. In the electron beam measurement experiments, current transformer NO.2 is located right behind the electron beam exit and in front of the entrance grid to determine the full value of the psedospark produced electron beam current I_1. The FC probe is located behind the entrance grid to determine the electron beam current I_2 passing through multiple grids to determine the attenuation coefficient $\frac{I_1}{I_2}$.

The vacuum and gas control system is also shown in Figure 6. The whole experimental system was evacuated to 10^{-5} Torr initially by a two-stage mechanical pump and turbo pump located at the anode side. The operating gas is argon. Argon gas enters into the vacuum system through a mass flow controller. The mass flow rate of argon can be adjusted accurately to control the operation pressure in the vacuum system. All the experimental data are acquired by a high speed oscilloscope with 500 MHz bandwidth and 1 GS/sec sampling rate. The control of the oscilloscope readout and data storage are accomplished by a LabVIEW software workbench. All the presented experimental results in Secs. III and IV represent the mean value over five repeated cycles.

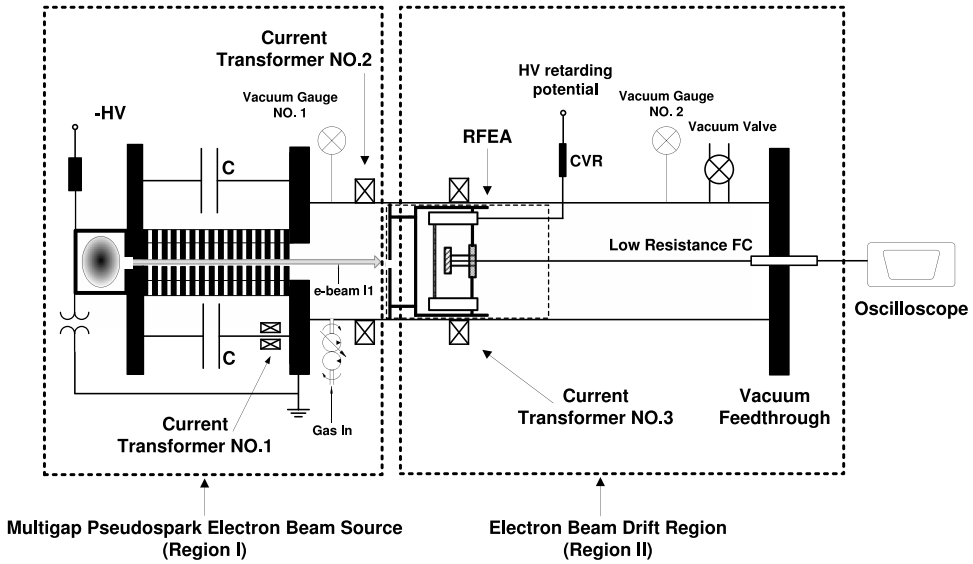

FIG. 6. Experimental setup of RFEA for the pseudospark-based electron beams.

III. EXPERIMENTAL RESULTS

In this section, three main experiments are conducted. First, the capability of the RFEA to hold high retarding potentials is validated by the leakage current tests in Section III A. In Section III B, the shunt resistance of the FC probe in the RFEA is determined, and its response time to pulses is validated by comparing with a calibrated current transformer probe. Finally, the attenuation coefficient of the RFEA is determined and calibrated in Section III C. In addition, the rise times of the electron beam pulse before and after attenuation are also presented and compared in this section.

A. Leakage current tests

As mentioned in Secs. I A and II A, the leakage current, which is formed between the retarding grid and ground, is mainly caused by gas breakdown under high retarding potentials (normally kV to tens of kV) and high pressure (10–100 mTorr). In order to validate the effect of the entrance grid to eliminate the gas breakdown and associated leakage current under high retarding potentials, the pressure values are measured by gauges located at region I (gauge NO.1) and region II (gauge NO.2) at given times, and the results are presented in Figure 7. As shown in Figure 7, when the pressure of the pseudospark-based electron source (region I) is ranging from 10^{-3}–10^{-2} Torr, the pressure of RPEA region (region II) can be maintained at 10^{-5} Torr. Additionally, the pressures in regions I and II under varying breakdown voltages of the pseudospark discharge are shown in Figure 8. As illustrated in Figure 8, the region II pressure is maintained at the high vacuum of 10^{-4}–10^{-5} Torr during the pseudospark discharge.

The leakage current flowing through the retarding grid is measured via the current viewing resistor (CVR) installed in the retarding power supply as illustrated in Figure 5. Under the retarding potentials ranging from 5 kV to 20 kV, the leakage current values measured in the retarding grid with and without the entrance grid are presented in Figure 9. It shows that there is current between the retarding grid and ground starting from 1 kV retarding potentials. The current flowing through the retarding grid is increased to 0.72 mA when the retarding potential goes up to 8.5 kV. The current (leakage current) between the retarding grid and ground is likely due to the charged particle production (ionization) within the gap between the retarding grid and grounded attenuation grid but may also be due to the surface conductivity along the insulators between the retarding grid and grounded grid. Without the entrance grid, the pressure within the RPEA (region II) is similar to the electron beam source (region I), that is, 10–100 mTorr. At this pressure and at 1–20 kV applied RPEA retarding potential, the electric field within the gap (0.5 –10 kV/mm) is near the minimum of the Paschen curve and generates a low-current DC glow discharge. For a gas discharge of this type, one would expect the discharge current to increase with the bias potential as shown in Figure 9. It is unclear how the presence of additional charged particles within the retarding field will affect the applied field and corresponding retardation of the electron beam. If the leakage current is carried by surface conductivity along insulators, it is also unclear how this current may affect the applied field. Fur-

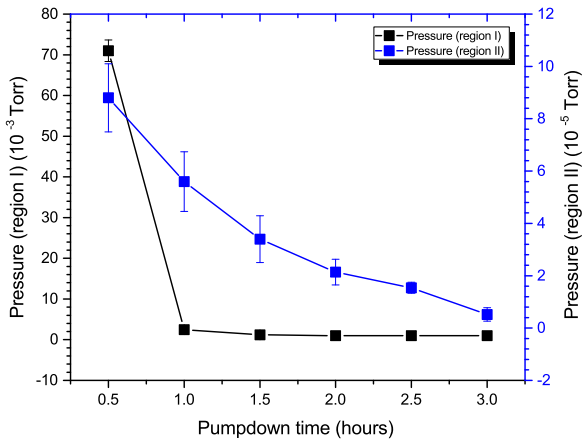

FIG. 7. Pressure values measured at regions I and II under varying pumpdown hours.

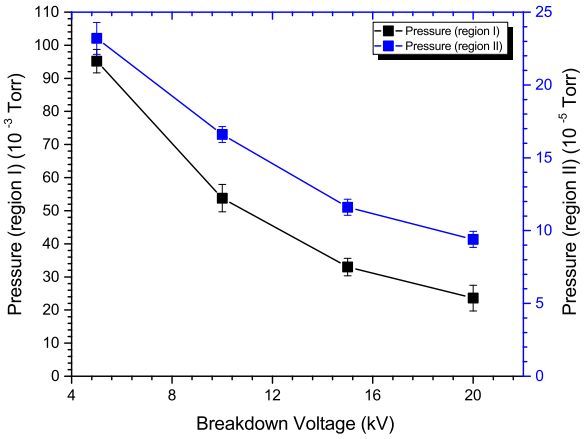

FIG. 8. Pressure values measured at regions I and II under varying breakdown voltages.

thermore, when the retarding potential is increased to higher value, the current will exceed the current limit of most high voltage power supply, which is normally 1–5 mA. Therefore operation within this regime, where significant leakage current is present, is to be avoided.

After the entrance grid is installed in front of the retarding grid and the pressure gradient is formed, the retarding potential can go up to 22 kV without any current as shown in Figure 9, validating that the improved RFEA can be operated successfully under retarding potentials up to 20 kV, which is the peak value of the pulsed electron beam accelerating potential in this work.

B. Performance validation of the FC probe

The objectives of the performance validation tests include the determination of probe shunt resistance and the available response time of the FC probe. The quantitative results of the FC probe performance are presented as the shunt resistance and response time to varying pulses generated by a calibrated pulse generator. Figure 11 shows the test layout of the FC probe performance validation tests, consisting of a pulse generator as the standard reference input signal, FC probe, and oscilloscope with 500 MHz bandwidth. Figure 10 shows the output signals from the FC probe and input signals from the pulse generator. The shunt resistance can be determined from the internal impedance of the pulse generator R_{in}, which is 50 Ω in the presented validation tests, and attenuation ratio of the FC probe, defined as the ratio of amplitude of output signal from FC to the amplitude of the source signal. As illustrated in Figure 11, the shunt resistance of the FC probe is calculated to be 0.086 Ω.

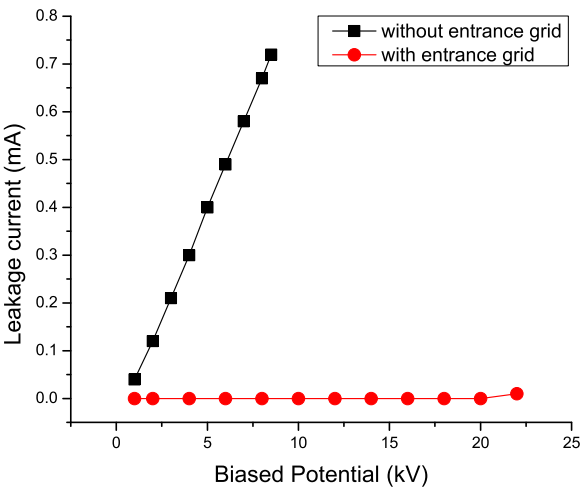

FIG. 9. Leakage currents flowing through the biased power supply.

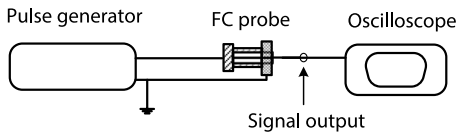

FIG. 10. Shunt resistance test setup.

The response time performance of the FC probe is determined via the fall time of a negative pulse signal passing through the FC probe. Figure 12 shows both the input signal from the pulse generator and the output signal from the FC probe. The input signal on the bottom has a 10.7 ns falling edge, while the output signal on the top displays a 12.8 ns falling edge. The response time error of the FC probe is defined as the magnitude of the difference between the fall time values of the FC signal and source signal divided by the fall time of the source. A value close to zero is desirable. The response time error values of the FC probe under the source fall time ranging from 8.6 to 80 ns are presented in Figure 13. As shown in Figure 13, the response time error has a maximum value of 19.7% at the fastest source fall time, 8.6 ns. As the source fall time is increased, the response time error is decreased below 10% at 25 ns and has a minimum value of 1.7% at 80 ns. In our research work, the fastest response time of the electron beam signal is greater than 50 ns. Thus the response time error of our probe is lower than 3.5% in our work.

C. Attenuation coefficient and space-charge limits

Attenuation of the electron beam is necessary for the RFEA to perform correctly: (1) The electron beam current

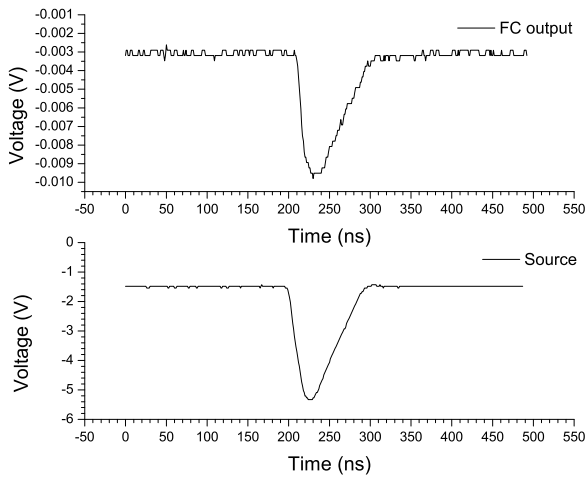

FIG. 11. Output signal from the FC probe (top) and source signal from the pulse generator (bottom).

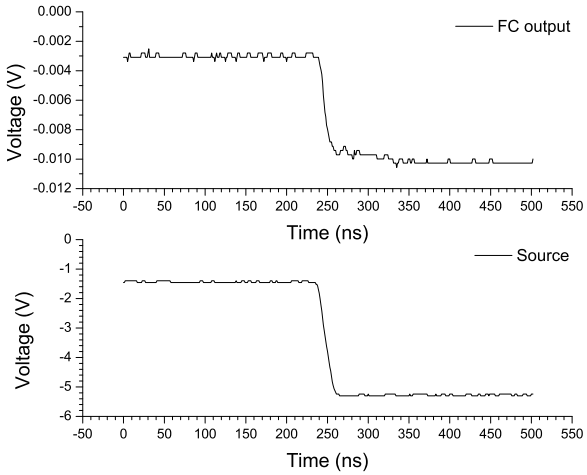

FIG. 12. Fall time of the FC probe output (top) and the source input signal (bottom).

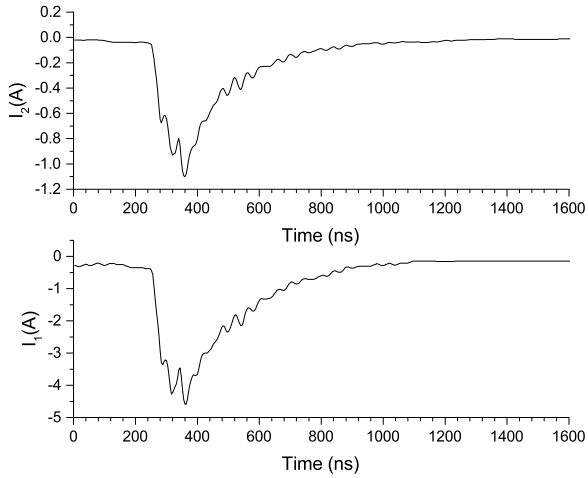

FIG. 14. Electron beam current before passing through the pin hole (bottom) and after passing through the pin hole (top) at 10 kV breakdown voltage.

density must be attenuated below the space-charge limit. (2) The electron beam current should decrease uniformly without causing distortion of the beam waveform. In our work, the attenuation of the electron beam current is due to both the entrance and attenuation grids.

Two electron beam current waveforms at 10 kV breakdown voltage are shown in Figure 14. The electron beam current exiting from the source I_1 is measured by a calibrated current transformer located in front of the entrance grid, with 100 MHz bandwidth and 10 ns usable rise time. The FC probe in RFEA is used to measure the attenuated electron beam current I_2, and the attenuation coefficient is determined by the scaling factor of $\frac{I_1}{I_2}$. As shown in Figure 14, the electron beam current I_1 is 4.6 A exceeding the space-charge limited value of 1.9 A at 10 kV. The attenuated electron beam current is 1.1 A, which yields a scaling factor of 4.2.

Additionally, the difference of the collected electron beam pulses before and after attenuation is also illustrated in Figure 14. The rise times of I_1 and I_2 are 108 ns and 104 ns, having an error percentage of 3.7%. However, the decay edge of the electron beam current mainly consists of "slow" electrons with energy lower than tens of eV,[10,11,35] which are easily defocused by the space-charge forces and distributed on the edge of the beam spot.[12,36,37] Thus this part of the distribution is easily intercepted by the entrance and attenuation grids. As illustrated in Figure 14, the decay times of I_1 and I_2 are 508 ns and 412 ns, with 18.9% error percentage, which is 5.1 times the rise time error. Thus compared with the slow decay tail of the electron beam pulse, the rise edge of electron beam pulse consisting of the high energy and medium energy electrons, which are the main focus of material processing applications, still preserve the time-resolved distributions when their amplitudes are attenuated.

Figure 15 shows the peak values of the attenuated electron beam currents under varying voltages of 5 kV, 10 kV, 15 kV, and 20 kV. In addition, the space-charge limited electron beam current values are also presented. The results demonstrate that by passing through multiple grids, the attenuated electron beam currents under breakdown voltages ranging from 5 kV to 20 kV are below the space-charge limited values.

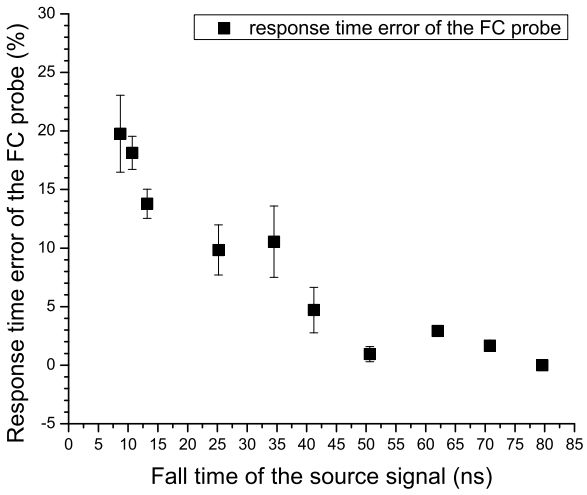

FIG. 13. Response time error of the FC probe.

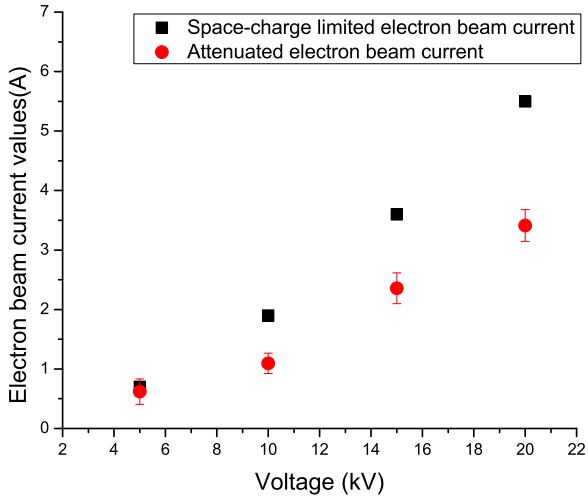

FIG. 15. Attenuated electron beam current and the calculated space-charge limited electron beam current.

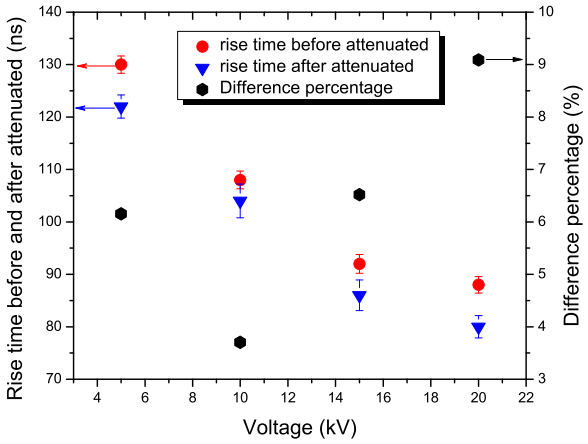

FIG. 16. Rise times of the collected electron beam pulses before and after attenuation.

The error percentages of the rise times between the electron beam pulses before and after attenuation (I_1 and I_2) are presented in Figure 16. The test results show that at all the breakdown voltages in this work, the error percentage is below 10%. The maximum rise time error of the electron beam pulse is obtained under 20 kV, which is 9.1%. At 10 kV, the minimum rise time error is only 3.7%.

D. Example of analyzer measurement

The RFEA developed in this work has been applied in the pseduspark-based electron beam measurements to determine the energy distributions of the THCD-based electron beams under various breakdown voltages. Figure 17 presents the electron beam pulses generated by 10 kV breakdown voltage and collected by the FC probe under retarding potentials ranging from 1 to 11 kV. As shown in Figure 17, under the low retarding potential, the collected electron beam pulse shows a fast rising edge and a slow and long tail. With the increase of the retarding potential, the amplitude of the collected electron current is decreased because more low energy electrons are stopped by the retarding field. The peak values of the electron beam pulses are located at 405 ns. As the retarding potential is increased from 1 kV to 11 kV, the peak of the electron beam current is decreased from 0.83 A to 0.26 A. For all of these experiments, the pressure in region II was always between 1.7×10^{-4} and 2.2×10^{-4} Torr.

Additionally, the electrons emitted at different times are retarded and attenuated with various magnitudes. Compared with the rise edge of the beam pulse, the long decay tail of the electron beam current is decreased more rapidly with increasing retarding potential. As shown in Figure 17, the electrons within 700–1200 ns have been stopped by the retarding grid. At 800 ns, the collected electron beam current is 0.28 A under 1 kV retarding potential. While the electron beam current collected at 800 ns under 11 kV retarding potential is only 0.04 A. However, at 360 ns and 400 ns, the collected electron beam currents under 11 kV retarding potential still remain 19.6% and 28.2% of the collected beam current under 1 kV retarding potential. Such variations suggest that the high energy electrons are mainly formed during the early phase on the rising edge of the emitted electron beam pulse starting from the

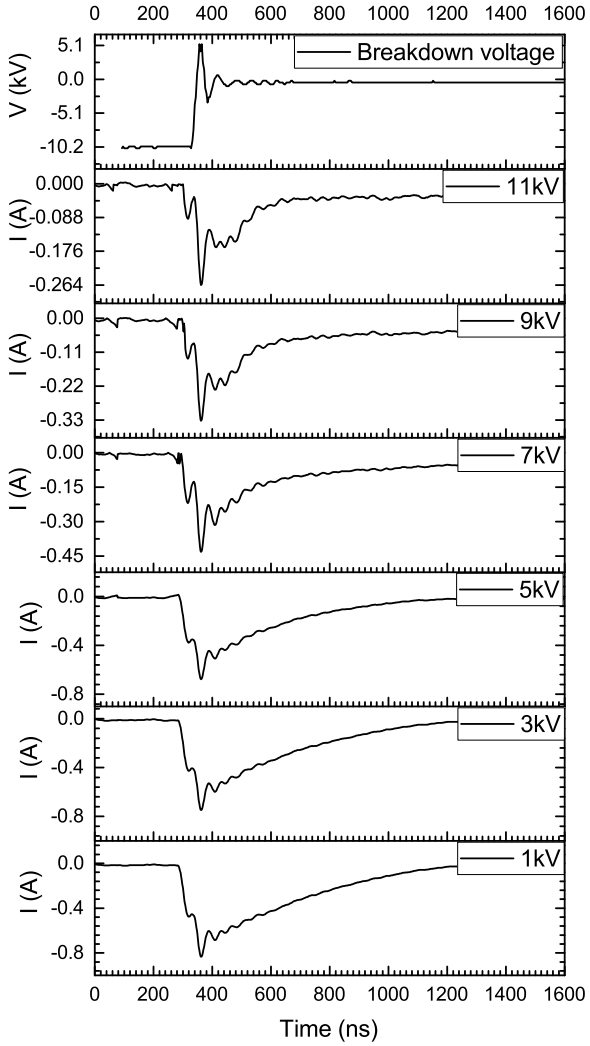

FIG. 17. Collected electron beam pulses with varying retarding potentials at 10 kV breakdown voltage.

ignition of gas breakdown in the THCD device. And the long decreasing tail of the electron beam pulse mainly consists of low energy electrons, which agrees with the previous research work presented in Refs. 10, 11, and 36. More results on the application of this RFEA in determining the time-resolved energy distribution and electron beam energy analysis have been published in Ref. 33.

IV. DISCUSSION AND CONCLUSIONS

The RFEA is essentially the only practical tool with which the time-resolved distribution of electron beam energy is measured. However, this technique is typically limited for electron beams generated in the "soft-vacuum" environment. Previous RFEA techniques have not been successful at measuring electron beam energy distributions for electron sources at high pressure. A major challenge has been the operation of the retarding grid at high potential in a high background pressure, which results in a glow discharge gas breakdown within the retarding grid gap region, thus skewing or masking the beam current. This article describes in detail a new RFEA probe constructed and tested specifically for electron beams with

energy up to 20 keV generated in a transient hollow cathode discharge (THCD), which is a common source of high energy pulsed electron beams. Here we have shown that a differentially pumped RFEA setup can capture the electron beam distribution of an electron source operating at high pressure. A strong pressure gradient can be maintained between the high-pressure electron source and low-pressure RFEA measurement region, thus allowing the RFEA to operate at high voltage, retard high-energy electrons, and thereby capture the energy distribution of emitted electrons. The performance of the RFEA is validated by three experiments on the retarding potential capacity, response time, and attenuation coefficient. The experimental results show that the retarding potential up to 22 kV can be obtained in the presented RFEA without any gas breakdown. And the fastest response time of the presented RFEA is 25 ns with error below 10%. In order to lower the high electron beam current density below the space-charge limit, an attenuation coefficient of 4.2 is obtained by careful design of the entrance and attenuation grids. The test results also show that the double grids do not affect the time-resolved distribution of the collected electron beam pulse after attenuation.

The RFEA can be used to determine the time-resolved energy distribution of pulsed electron beams generated by the pseudospark discharge operating between 5 and 20 kV breakdown voltages. Applications of this technique demonstrate that in addition to the time-resolved energy spectra, particle numbers of electrons at various energy groups and electron beam energy transformation efficiency can be determined also.[33] The results are applicable to the theoretical modeling of the pulsed electron beam transportation in plasma and its interactions with the metallic material.[1,38,39] It may also be applicable to other high power pulsed discharge experiments with the proper adjustment of the grids according to the methods presented in this paper, with the proper RFEA design according to the methods presented in this paper. Specific design considerations include using an entrance grid or orifice to establish a 10^2 pressure differential between the beam source and RFEA and sizing the attenuation grid to reduce the beam current below the space-charge limit. In practice, the RFEA measurement setup can be replaced with the desired processing application, e.g., surface modification. If the electron source is applied as demonstrated here, where the electron source is in the high-pressure region and processing setup is in the low-pressure region, then the electron beam impinging on the target is as measured by the RFEA. However, if the electron source and processing setup are both at high-pressure, then the electron beam may be modified by the presence of additional background gas. These effects may need to be accounted for depending on the specific application.

ACKNOWLEDGMENTS

This work was sponsored by the Shanghai Pujiang Program (Grant No. 15PJ1403600) and the National Natural Science Foundation of China (Grant No. 51505285).

[1]L. Jiang and H. L. Tsai, Int. J. Heat Mass Transfer **48**, 487–499 (2005).
[2]I. H. Chowdhury and X. Xu, Numer. Heat Transfer, Part A **44**(3), 219–232 (2003).
[3]V. Surla and D. Ruzic, J. Phys. D: Appl. Phys. **44**(17), 174026 (2011).
[4]L. E. Murr, S. M. Gaytan, D. A. Ramirez, E. Martinez, J. Hernandez, K. N. Amato, P. W. Shindo, F. R. Medina, and R. B. Wicker, J. Mater. Sci. Technol. **28**(1), 1–14 (2012).
[5]R. A. Dugdale, J. Mater. Sci. **10**(5), 896–904 (1975).
[6]R. Stark, J. Christiansen, K. Frank, F. Mücke, and M. Stetter, IEEE Trans. Plasma Sci. **23**(3), 258–264 (1995).
[7]D. I. Proskurovsky, V. P. Rotshtein, G. E. Ozur, A. B. Markov, D. S. Nazarov, M. A. Shulov, Yu. F. Ivanov, and R. G. Buchheit, J. Vac. Sci. Technol., A **16**(4), 2480–2488 (1998).
[8]D. I. Proskurovsky, V. P. Rotshtein, G. E. Ozur, Y. F. Ivanov, and A. B. Markov, Surf. Coat. Technol. **125**, 49–56 (2000).
[9]K. Frank and J. Christiansen, IEEE Trans. Plasma Sci. **17**(5), 748–753 (1989).
[10]E. Dewald, K. Frank, D. H. H. Hoffmann, R. Stark, M. Ganciu, B. N. Mandache, M. G. Nistor, A.-M. Pointu, and I.-I. Popescu, IEEE Trans. Plasma Sci. **25**, 272–278 (1997).
[11]E. Dewald, K. Frank, D. H. H. Hoffmann, and A. Tauschwitz, IEEE Trans. Plasma Sci. **30**, 363–374 (2002).
[12]K. Ramaswamy, W. W. Destler, and J. Rodgers, J. Appl. Phys. **75**(9), 4432–4437 (1994).
[13]G. Modreanu, N. B. Mandache, A. M. Pointu, M. Ganciu, and I. I. Popescu, J. Phys. D: Appl. Phys. **33**, 819–825 (2000).
[14]R. Kowalewicz and T. Redel, IEEE Trans. Plasma Sci. **23**(3), 270–274 (1995).
[15]R. F. Fernsler, R. F. Hubbard, and M. Lampe, J. Appl. Phys. **75**(7), 3278–3293 (1994).
[16]A. W. Molvik, Rev. Sci. Instrum. **52**(5), 704–711 (1981).
[17]Y. Zou, Y. Cui, I. Haber, M. Reiser, and P. G. O'shea, Phys. Rev. Spec. Top.–Accel. Beams **6**, 1–10 (2003).
[18]P. Gill and C. E. Webb, J. Phys. D: Appl. Phys. **10**(3), 299–301 (1977).
[19]K. Takahashi, C. Charles, R. W. Boswell, T. Kaneko, and R. Hatakeyama, Phys. Plasmas **14**(11), 114503 (2007).
[20]R. A. Pitts, R. Chavan, S. J. Davies, S. K. Erents, G. Kaveney, G. F. Matthews, G. Nelll, J. E. Vince, and I. Duran, Rev. Sci. Instrum. **74**(11), 4644–4657 (2003).
[21]D. Gahan, B. Dolinaj, and M. B. Hopkins, Rev. Sci. Instrum. **79**(3), 033502 (2008).
[22]J. L. Rovey and A. D. Gallimore, Phys. Plasmas **14**(3), 033505 (2007).
[23]Y. Uno, A. Okada, K. Uemura, P. Raharjo, T. Furukawa, and K. Karato, Precis. Eng. **29**(4), 449–455 (2005).
[24]A. Okada, R. Kitada, Y. Okamoto, and Y. Uno, CIRP Ann.-Manuf. Technol. **60**(1), 575–578 (2011).
[25]A. Okada, Y. Uno, N. Yabushita, K. Uemura, and P. Raharjo, J. Mater. Process. Technol. **149**, 506–511 (2004).
[26]H. Bluhm, *Pulsed Power Systems: Principles and Applications* (Springer-Verlag, Berlin, Heidelberg, 2006), pp. 135–137.
[27]J. H. Moore, C. D. Christopher, A. C. Michael, and C. G. Sandra, *Building Scientific Apparatus* (Cambridge University Press, New York, 2009), pp. 97–98.
[28]Yu. D. Korolev and K. Frank, IEEE Trans. Plasma Sci. **27**(5), 1525–1537 (1999).
[29]A. V. Kozyrev, Yu. D. Korolev, V. G. Rabotkin, and I. A. Shemyakin, J. Appl. Phys. **74**(9), 5366–5371 (1993).
[30]G. Schaefer, M. Kristiansen, and A. Guenther, *Gas Discharge Closing Switches* (Plenum Press, New York, N.Y., 1990), Vol. 6, pp. 306–307.
[31]H. Bluhm, *Pulsed Power Systems: Principles and Applications* (Springer-Verlag, Berlin, Heidelberg, 2006), pp. 259–260.
[32]H. Chuaqui, M. Favre, E. Wyndham, L. Arroyo, and P. Choi, Rev. Sci. Instrum. **60**(1), 141–142 (1989).
[33]J. Hu and J. L. Rovey, J. Appl. Phys. **114**(7), 073301 (2013).
[34]J. Hu and J. L. Rovey, J. Phys. D: Appl. Phys. **45**(46), 465203 (2012).
[35]C. Jiang, A. Kuthi, M. A. Gundersen, and W. Hartmann, Appl. Phys. Lett. **87**, 131501 (2005).
[36]W. W. Destler, Z. Segalov, J. Rodgers, K. Ramaswamy, and M. Reiser, Appl. Phys. Lett. **62**(15), 1739–1741 (1993).
[37]C. J. Liu and M. J. Rhee, Proc. IEEE Part. Accel. Conf. **1**, 688–690 (1993).
[38]J. A. Sanchez and M. Pinar Mengü, J. Appl. Phys. **103**(5), 054316 (2008).
[39]B. Dikshit, G. R. Zende, M. S. Bhatia, and B. M. Suri, IEEE Trans. Plasma Sci. **37**(7), 1196–1202 (2009).